Biosensors and Bioelectronics 65 (2015) 115–120

Contents lists available at ScienceDirect

Biosensors and Bioelectronics

journal homepage: www.elsevier.com/locate/bios

A highly selective photoelectrochemical biosensor for uric acid based on core–shell Fe_3O_4@C nanoparticle and molecularly imprinted TiO_2

Chunjing Zhang [a,b], Shihui Si [a,*], Zhengpeng Yang [b]

[a] College of Chemistry and Chemical Engineering, Central South University, Changsha 410083, China
[b] Institute of Materials Science and Engineering, Henan Polytechnic University, Jiaozuo 454000, China

ARTICLE INFO

Article history:
Received 1 July 2014
Received in revised form
4 October 2014
Accepted 7 October 2014
Available online 16 October 2014

Keywords:
Photoelectrochemical biosensor
Uric acid
Fe_3O_4@C
Molecularly imprinted TiO_2
Magnetic electrode

ABSTRACT

Combining the surface modification and molecular imprinting technique, a novel photoelectrochemical sensing platform with excellent photochemical catalysis and molecular recognition capabilities was established for the detection of uric acid based on the magnetic immobilization of Fe_3O_4@C nanoparticles onto magnetic glassy carbon electrode (MGCE) and modification of molecularly imprinted TiO_2 film on Fe_3O_4@C. The developed biosensor was highly sensitive to uric acid in solutions, with a linear range from 0.3 to 34 μM and a limit of detection of 0.02 μM. Furthermore, the biosensor exhibited outstanding selectivity while used in coexisting systems containing various interferents with high concentration. The practical application of the biosensor was also realized for the selective detection of uric acid in spiked samples. The study made a successful attempt in the development of highly selective and sensitive photoelectrochemical biosensor for urine monitoring.

1. Introduction

Uric acid (UA), a primary final product of purine metabolism, is a key biomarker for the diagnosis of several diseases such as gout, Lesch–Nyhan syndrome, hyperuricemia, leukemia and so on (Li et al., 2012). Therefore, the monitoring of UA in human blood and urine is very important for the prevention of the mentioned and other similar diseases. Various techniques have been developed for UA detection, such as enzymatic assay (Piermarini et al., 2013), high-performance liquid chromatography (HPLC) (Kaňďár et al., 2011), mass spectrometry (Siekmann, 1985), capillary electrophoresis (CE) (Pormsila et al., 2009), chemiluminescence (Chaudhari et al., 2012), colorimetry (Miller and Oberholzer, 1990) and electrochemistry (Zhang and Yin, 2014; Guan et al., 2014). Despite many advances in UA detection, the sensitive, selective, stable and facile methods still need to be explored until now.

Photoelectrochemical measurement based on the electron transfer among analyte, photoactive species and electrode with photoirradiation is a newly and promising analytical technique for sensing application (Tu et al., 2010; Wang et al., 2009). In photoelectrochemical sensing, light is used to excite active species on the electrode, and the interaction between analytes and the illuminated photoelectrochemically active materials induces photocurrent change of the photoelectrochemical active species modified electrode. Coupling photoirradiation with electrochemical detection, the method exhibits the properties of both optical methods and electrochemical sensors (Zhang et al., 2013). Due to its separation of the excitation source and detection signal, the photoelectrochemical analysis possesses several advantages such as high sensitivity, low background signal, low cost and easy miniaturization of detection devices (Wang et al., 2014a, 2014b). The photoelectrochemical sensors have drawn growing interest in analytical chemistry, and have been utilized for sensitive analysis of target molecules and ions (Sun et al., 2013; Zhang et al., 2014; Jeon et al., 2013). Still, the photocatalytic oxidation lacks selectivity due to the nature of hydroxyl radicals or holes generated in photocatalytic oxidation, and is not suitable for selective analysis (Shi et al., 2011). Therefore, how to realize the selectivity of a photoelectrochemical sensor is a quite critical issue. Molecular imprinting technique, the design and construction of mimetic receptor system with predetermined recognition for target molecule, has been proposed and developed rapidly (Yang and Zhang, 2011, 2013). Recently, the photoelectrochemical sensors based on molecularly imprinted polymer have been fabricated, and exhibited a favorable selectivity towards template molecules (Sun et al., 2014; Tran et al., 2014; Wang et al., 2013).

In this work, Fe_3O_4@C nanoparticles and molecularly imprinted TiO_2 (MIT) were employed as carrier and sensing film, respectively. A novel photoelectrochemical biosensor with excellent photochemical catalysis and molecular recognition capabilities was fabricated for UA detection based on the magnetic immobilization of Fe_3O_4@C nanoparticles onto the MGCE and modification of MIT

* Corresponding author. Fax: +86 731 88879616.
E-mail address: shihuisi2013@163.com (S. Si).

http://dx.doi.org/10.1016/j.bios.2014.10.013
0956-5663/

film on Fe_3O_4@C. The core–shell Fe_3O_4@C nanoparticles possess good magnetism and conductivity, which can facilitate the strong binding of carrier to the electrode and enhance the photocurrent (Zhang and Kong, 2011; Liu et al., 2014) due to its fast electron-transfer capability. The MIT is not only an outstanding photochemical catalyst with high surface area, structural rigidity, excellent stability and biocompatibility, but also can selectivity capture the target molecules (Yang et al., 2011; Luo et al., 2013). All these characteristics would lead to an excellent photoelectrochemical biosensor with high sensitivity, selectivity and stability.

2. Experimental

2.1. Materials and apparatus

$FeCl_2 \cdot 4H_2O$, $FeCl_3 \cdot 6H_2O$, NH_4OH solution (25%) and benzoquinone (BQ) were of analytical grade and obtained from Shanghai Chemical Reagent Co. Ti(O-^{n}Bu)$_4$ was purchased from Sigma Chem. Co. and used as received. Glucose, UA, ascorbic acid (AA), glutamic acid (GA), cytosine, purine and urea were purchased from Shanghai Aladdin Chemical Co., China. All other chemicals were of analytical grade and used without further purification. Deionized (DI) water (resistivity of 18 MΩ cm) was obtained from a Millipore Milli-Q Water System (Millipore Inc.), and was used for rinsing and for makeup of all aqueous solutions.

Transmission electron microscopy (TEM) analysis was performed on a JEOL 2100F electron microscope (Japan) at an accelerating voltage of 200 kV. Scanning electron micrograph (SEM) was conducted on a Hitachi S-520 scanning electron microscope (Hitachi Ltd., Tokyo, Japan) working at 20 kV. X-ray diffraction (XRD) was performed on a Rigaku D/MAX-RCX-ray diffractometer using Cu Kα radiation. Infrared (IR) spectra were recorded on Nicolet 200SXV Fourier transform infrared (FTIR) spectrometer using a KBr wafer. The magnetization measurements were performed at room temperature using model 155 vibrating magnetometer. The chromatographic analysis was performed in High Performance Liquid Chromatography (HPLC) system equipped with a variable-wavelength ultraviolet (UV) detector and an automatic injector (LC-10 VP, Shimadzu Scientific Instrument, Kyoto, Japan). A 320 W low-pressure mercury lamp (Philips, 254 nm) was used as UV irradiation source. All electrochemical experiments were carried out on CHI660c workstation (CH Instrument, USA).

2.2. Design and fabrication of the UA photoelectrochemical biosensor

The preparation of Fe_3O_4@C nanoparticles were conducted according to the previous reports with some modification (Zhang and Kong, 2011). Briefly, 25% NH_4OH solution (10 mL) was slowly dropped into a 30 mL aqueous solution containing 1.85 mmol $FeCl_2 \cdot 4H_2O$ and 3.7 mmol $FeCl_3 \cdot 6H_2O$ in N_2 atmosphere under vigorous stirring. After incubation for 30 min at 80 °C, the resultant ultrafine magnetic particles were collected by magnetic decantation, washed several times with DI water, and then vacuum dried at 60 °C for 4 h. The as-prepared Fe_3O_4 nanoparticles (50 mg) were dispersed in a 0.1 M HNO_3 solution for 10 min, followed by washing several times in DI water. Subsequently, the treated magnetic nanoparticles were introduced into 0.3 M aqueous glucose solution (15 mL). After vigorous stirring for 20 min, the solution was sealed in a Teflon-line autoclave. The autoclave was kept at 180 °C for 6 h, and then cooled naturally. The resultant products were separated by a magnet and washed in DI water and ethanol. Finally, dried at 60 °C, stand by to application.

The MGCE was prepared and treated according to our previous work (Yang et al., 2014). 2.0 mL aqueous suspension of Fe_3O_4@C (0.3 mg mL^{-1}) was dripped onto the obtained MGCE (10 mm in diameter), the solid Fe_3O_4@C nanoparticles were magnetically attracted down to the electrode surface immediately from the suspension. Thus, Fe_3O_4@C modified MGCE was fabricated.

The formation of MIT film on Fe_3O_4@C modified MGCE was performed by sol–gel hydrolysis of Ti(O-^{n}Bu)$_4$ followed by extraction and heat treatment. Specifically, Ti(O-^{n}Bu)$_4$ (0.8 mmol) and UA (0.3 mmol) were dissolved in 10 mL of toluene–ethanol (v/v, 2:1) mixture, and then vigorously stirred at room temperature. Subsequently, the solution was diluted by 20 times with water-saturated toluene and continuously stirred for 6 h to get a sol–gel solution which was used as a dipping solution. The Fe_3O_4@C modified MGCE was immersed into the dipping solution for 8 min at room temperature, rinsed with toluene, hydrolyzed in water and dried in N_2 atmosphere. The "dipping-rinse-hydrolyzation-drying"cycle was repeated two times, and then the Fe_3O_4@C modified MGCE whose surface was covered with a TiO_2 layer containing the template molecule of UA was obtained. Finally, the template UA molecules were completely removed from the modified layer by multiple extractions ($n=8$, extraction time 10 min) with 10 mL hot water (ca. 80 °C). After heat treatment at 200 °C in N_2 atmosphere for 4 h, the MIT modified electrode was obtained and denoted as Fe_3O_4@C@MIT modified MGCE. Thus, the UA photoelectrochemical biosensor was fabricated. The obtained biosensor was stored dry at room temperature for future use. For comparison, the formation of non-imprinted TiO_2 on Fe_3O_4@C modified MGCE was conducted using a similar procedure without template molecules, and was denoted as Fe_3O_4@C@TiO_2 modified MGCE.

2.3. Photoelectrochemical measurements

All photoelectrochemical measurements were performed in a three-electrode cell configuration with Fe_3O_4@C@MIT or Fe_3O_4@C@TiO_2 modified MGCE as the working electrode, a saturated calomel electrode as the reference electrode, and a Pt wire counter electrode. After the electrodes were incubated in 0.1 M phosphate buffer solution (PBS, pH 7.4) containing different concentration of UA for 10 min under stirring, the UV illumination was conducted and the photocurrent was generated due to photocatalytical oxidization of UA. *I–t* curve was used for sensitivity, selectivity, stability and detection experiments.

3. Results and discussion

3.1. Fabrication and characterization of the UA photoelectrochemical biosensor

The route of design and fabrication of the UA photoelectrochemical biosensor was shown in Fig. 1 A. Fe_3O_4 nanoparticles were prepared by co-precipitation of Fe^{2+} and Fe^{3+} ions in ammonia solution. The carbon layer was formed at the surface of Fe_3O_4 nanoparticles by the hydrothermal reaction in aqueous glucose solution. The as-formed core–shell Fe_3O_4@C nanoparticles were modified onto the MGCE surface by magnetic force. The molecularly imprinted TiO_2 was functionalized on the Fe_3O_4@C modified MGCE by the sol–gel hydrolysis of Ti(O-^{n}Bu)$_4$ in the presence of the template molecules UA. UA was embedded in TiO_2 film by strong hydrogen bond formed between N–H groups of UA and hydroxyl groups of TiO_2. After removal of UA, recognition sites complementary to the molecular shape, size and functionality of UA were formed in TiO_2 film which would efficiently and selectively rebind UA in solution. The morphology of the as-prepared samples was investigated by TEM (Supplementary information Fig. S1). As presented in Fig. S1a, the Fe_3O_4@C microspheres showed a

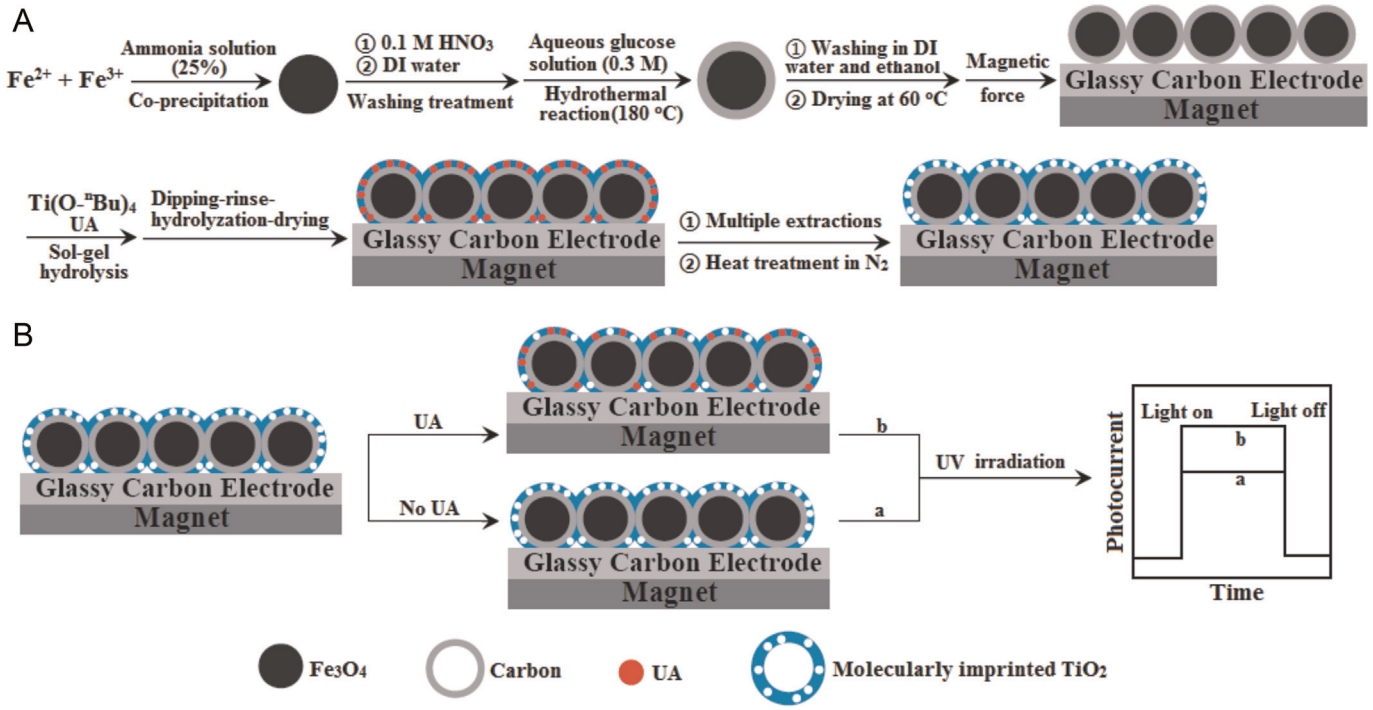

Fig. 1. Schematic illustration for (A) fabrication and (B) detection mechanism of the UA photoelectrochemical biosensor.

core–shell structure in which the black Fe_3O_4 particles were encapsulated into thin gray carbon shells ca. 2.0 nm in thickness. The obtained Fe_3O_4@C@TiO_2 and Fe_3O_4@C@MIT also possessed monodispersed spherical morphology as shown in Fig. S1b and c, a uniform TiO_2 layer (bright, ~5.2 nm in thickness) was formed on individual Fe_3O_4@C particle. From the enlarged TEM images (the

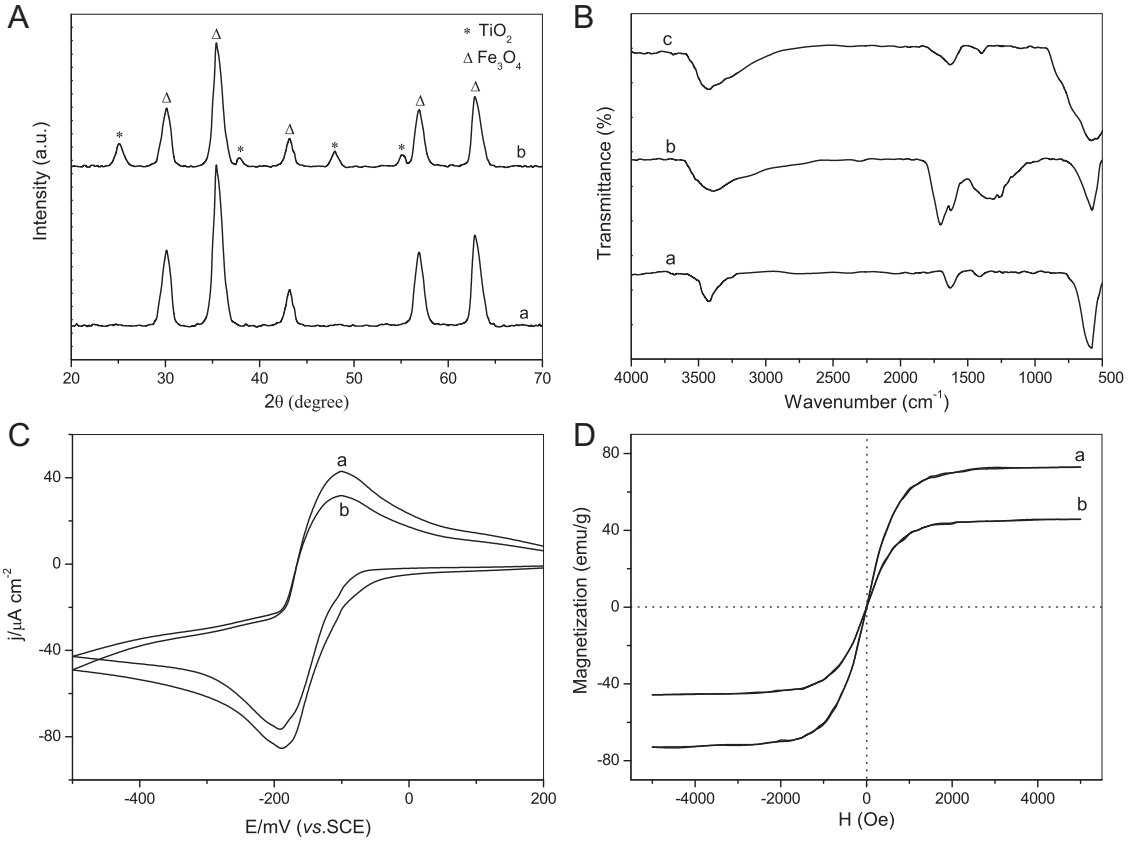

Fig. 2. (A) XRD patterns of (a) Fe_3O_4 and (b) Fe_3O_4@C@MIT. (B) FTIR spectra of (a) Fe_3O_4, (b) Fe_3O_4@C and (c) Fe_3O_4@C@MIT. (C) Cyclic voltammograms of 3.0 mM BQ in 0.1 M KCl aqueous solution on Fe_3O_4@C@MIT modified MGCE (a) and Fe_3O_4@C@TiO_2 modified MGCE (b). $v = 100$ mV s^{-1}. (D) Room temperature field-dependent magnetization curves of (a) Fe_3O_4 and (b) Fe_3O_4@C.

insets in Fig. S1b and c), the Fe_3O_4@C@MIT clearly exhibited porous TiO_2 shell compared to the Fe_3O_4@C@TiO_2. The morphology of Fe_3O_4@C@MIT modified MGCE was examined by SEM (Supplementary information Fig. S2). The electrode surface was actually rather rough, and was composed of closely packed nanometer sized spherical grains which were remarkably uniform with an average size of about 26 nm in the diameter.

The composition and crystal structure of Fe_3O_4@C@MIT were identified by XRD, and for a comparison, the XRD pattern of Fe_3O_4 was also analyzed. As seen in Fig. 2A, the diffraction peaks at $2\theta = 30.1°$, 35.2°, 43.0°, 56.8° and 62.3° can be perfectly indexed to those XRD patterns of Fe_3O_4 nanoparticles (Yang et al., 2010), indicating a cubic spinel structure of magnetite. No diffraction peaks of carbon could be observed in the spectra of Fe_3O_4@C@MIT, which suggested that carbonaceous coating outside Fe_3O_4 nanoparticles was amorphous, and retained a small presence compared with Fe_3O_4. Compared with diffraction peaks of Fe_3O_4, some relatively weak diffraction peaks appeared at $2\theta = 25.1°$, 38.1°, 48.0° and 54.9°, revealing the formation of thin-layer anatase TiO_2 on the Fe_3O_4@C nanoparticles. Additionally, the peak intensity of Fe_3O_4 in Fe_3O_4@C@MIT was slightly weakened, which further confirmed the existence of carbon and TiO_2 with low content in the outlayer of nanospheres.

FTIR analysis was performed on Fe_3O_4, Fe_3O_4@C and Fe_3O_4 @C@MIT samples to further prove the sequential coating of carbon and MIT layers on the magnetite particle. Fig. 2B shows their FTIR spectra recorded in the range of 4000–500 cm^{-1}. In three curves, the bands centered at ca. 1629 and 3427 cm^{-1} can be assigned to the O–H stretching modes and bending vibration, respectively (Rahman et al., 2009). In the curve (a), the high-intensity band at 578 cm^{-1} corresponds to the Fe–O stretching vibration from the magnetite phase (Yang et al., 2010). In the curve (b), the band at 578 cm^{-1} for Fe_3O_4 was obviously weakened and several new bands corresponding to the carbon were clearly observed. The high-intensity bands at ca. 1700 cm^{-1} and 1622 cm^{-1} can be attributed to C=O and C=C vibrations respectively, and the enhanced hydroxyl peak at ca. 3427 cm^{-1} implied a successful immobilization of carbon with the hydrophilic functional groups on Fe_3O_4 nanoparticles. In the curve (c), a strong band in the range from 528–900 cm^{-1} relating to the stretching vibration of Ti–O–Ti bond was clearly observed, indicating the formation of TiO_2 in the outlayer of Fe_3O_4@C@MIT. The bands for Fe_3O_4@C@MIT, belonging to the hydrophilic groups of the carbon layer, were significantly weakened. Especially, the peak intensity ratio of C=O vibration to C=C vibration was largely decreased after TiO_2 deposition on the carbon surface, which may be related to the formation of C–O–Ti from C=O (Liu et al., 2014), suggesting a strong interaction at the interface of carbon and TiO_2.

The formation of MIT film on the Fe_3O_4@C surface was evaluated using electrochemical measurements. Fig. 2C shows cyclic voltammograms (CV) of 3.0 mM BQ in 0.1 M KCl aqueous solution on Fe_3O_4@C@MIT and Fe_3O_4@C@TiO_2 modified MGCEs. The profiles were almost similar expect for the difference of peak current density, indicating two kinds of different films on the Fe_3O_4@C surface. The peak current density on Fe_3O_4@C@MIT modified MGCE was obviously higher than that on Fe_3O_4@C@TiO_2 modified MGCE. The enhanced peak current can be attributed to the change of surface/inner structure of TiO_2 film caused by molecular imprinting, enhancing porosity of TiO_2 film and resulting in faster BQ diffusion through the film to the carbon surface. Thus, CV measurements confirm strongly the existence of MIT film on the Fe_3O_4 @C surface.

The magnetic property of as-prepared Fe_3O_4 and Fe_3O_4@C were quantified by vibrating sample magnetometer at room temperature. Fig. 2D shows the magnetization–hysteresis loops of samples with different composition. The magnetic saturation (Ms) for

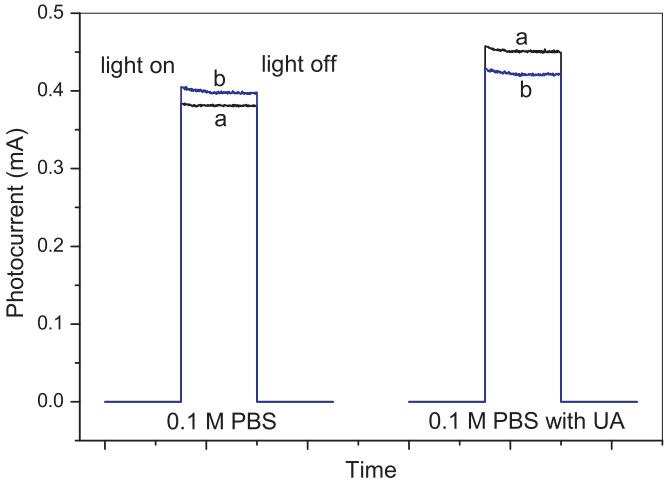

Fig. 3. Photocurrent responses of (a) Fe_3O_4@C@MIT modified MGCE and (b) Fe_3O_4@C@TiO_2 modified MGCE in 0.1 M PBS (pH 7.4) without and with 6 μM UA.

Fe_3O_4 was 72.9 emu/g, and that of Fe_3O_4@C was 45.7 emu/g. The decrease in Ms can be attributed to the introduction of nonmagnetic carbon shell on the Fe_3O_4 surface, which will quench the magnetic moment. Additionally, it was observed that the magnetization and demagnetization curves were coincidence, no hysteresis phenomenon existed, and remanent magnetization and coercivity were equal to zero. Significantly, the results indicate that the obtained Fe_3O_4@C nanoparticles possess strong magnetization and superparamagnetism, which are advantageous to the fabrication of the photoelectrochemical biosensor.

Fig. 3 shows the photocurrent responses of Fe_3O_4@C@MIT and Fe_3O_4@C@TiO_2 modified MGCEs in 0.1 M PBS (pH 7.4) without and with 6 μM UA. The photocurrent responses of the two electrodes in PBS were approximate, and reached relatively high values. This may result from the existence of conductive carbon interlayer between Fe_3O_4 and TiO_2, which can accelerate the electron transfer, lower the recombination of photogenerated electrons–holes and enhance the photoelectric conversion efficiency. The photocurrent responses of the two electrodes were evidently enhanced in the presence of UA compared to that in PBS, the photocurrents of Fe_3O_4@C@MIT and Fe_3O_4@C@TiO_2 modified MGCEs increased 18.35% and 5.79%, respectively. The larger enhanced photocurrent on Fe_3O_4@C@MIT modified MGCE can be attributed to the presence of MIT film on Fe_3O_4@C. As shown in Fig. 1B, the imprinted sites on the surface of Fe_3O_4@C@MIT modified MGCE can specifically rebind and accumulate UA molecules on the electrode surface. As a result, more UA molecules were photocatalytically oxidized on the Fe_3O_4@C@MIT modified MGCE, causing a stronger photocurrent. It not only embodies the excellent selectivity of MIT, but also suggests that molecular recognition and accumulation will greatly improve the sensitivity of the biosensor.

3.2. Biosensing performance

The photocurrent response of the photoelectrochemical biosensor to UA was performed in 0.1 M PBS (pH 7.4) containing different concentration of UA. As seen in Fig. 4A and B, the photocurrent increased linearly with the concentration of UA in the range of 0.3–34 μM. The linear regression equation was I (mA) = 0.4184 + 0.0039 C (μM) with a correlation coefficient of 0.9989. The limit of detection (LOD) was estimated to be 0.02 μM (S/N = 3), which was lower than that of previous methods (Zhang and Yin, 2014; Chen et al., 2010). Moreover, the response could reach a steady signal within only 1s. Obviously, the proposed

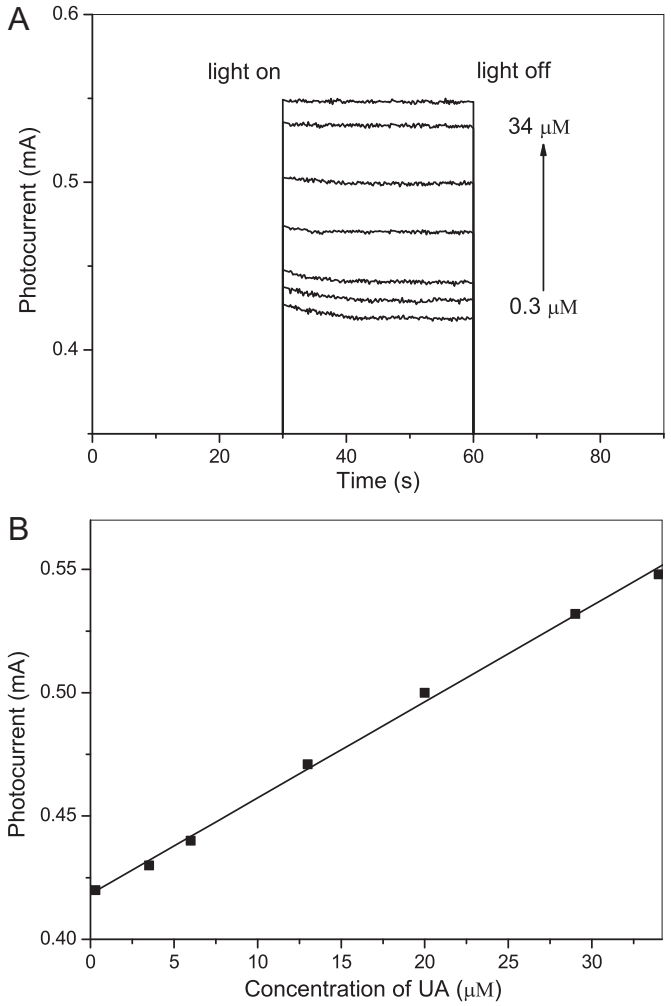

Fig. 4. (A) Photocurrent responses of Fe_3O_4@C@MIT modified MGCE in 0.1 M PBS (pH 7.4) in the presence of 0.3, 3.5, 6, 13, 20, 29 and 34 μM UA (from bottom to top). (B) Linear calibration curve. All photocurrents were recorded after the electrodes were immersed in the UA solution for 10 min.

photoelectrochemical biosensor shows promise for application in the monitoring of UA with its low LOD and short response time.

The molecular recognition capability of the photoelectrochemical biosensor was investigated by employing AA, GA, cytosine, glucose, purine and urea coexisting in urine as interfering substances. The selectivity was evaluated by calculating the photocurrent ratio (PI/PI_0). Herein, PI_0 was the photocurrent for 6 μM UA (S0) and was set as 100%, while PI referred to the photocurrent of the two-component system containing 6 μM UA and 50 μM interfering substances (S1–S6). As seen in Fig. 5, the photocurrent showed a slight increase and the deviations were all less than 2.5% even the concentrations of the interfering substances were 8.3 times that of UA, which adequately revealed that this photoelectrochemical biosensor presented a superior selectivity towards UA. The outstanding selectivity of the biosensor can be mainly attributed to the recognition function of surface molecularly imprinted modification, the large quantities and high qualities of imprinted sites provided by Fe_3O_4@C@MIT. The imprinted cavities formed in MIT film can distinguish UA from other species through molecular size and functional group distribution, and rebind UA selectively by hydrogen bonds interaction. Thus, UA molecules were specifically accumulated on the biosensor surface, whereas other coexistent molecules not complementary to the cavities hardly interacted with the biosensor and mainly remained in the bulk solution.

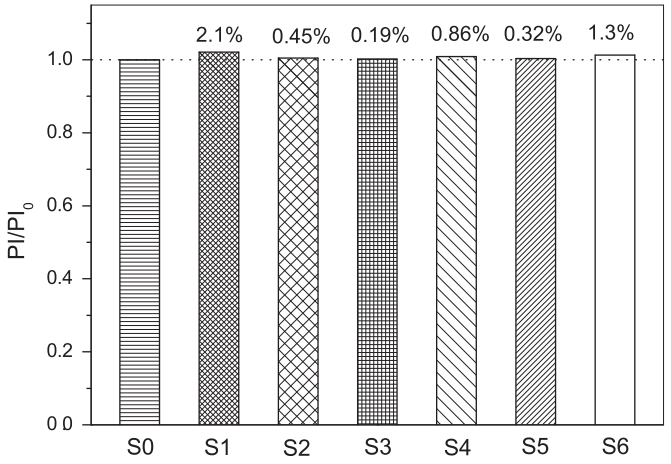

Fig. 5. Photocurrent ratio of Fe_3O_4@C@MIT modified MGCE in 0.1 M PBS (pH 7.4) containing 6 μM UA in the absence (PI_0) and presence (PI) of 50 μM AA (S1), GA (S2), cytosine (S3), glucose (S4), purine (S5) and urea (S6), respectively.

To investigate the reproducibility of the biosensor, the photocurrent responses were performed in 0.3, 3.5, 6, 13, 20, 29 and 34 μM UA using five different electrodes, respectively. These electrodes were prepared under the same conditions, and then were used to detect the same UA solution. The calculated relative standard deviation (RSD) for all concentrations was lower than 4.0%. The repeatability of the proposed method was examined by detecting the photocurrent responses of the aforementioned UA with the same electrode. RSD of photocurrent changes for all UA concentrations was lower than 3.2% ($n=5$). Furthermore, the biosensor could be used many times, and the photocurrent remained stable after 20 continuous measurements of 6 μM UA with a RSD of 2.1%. The long-term stability revealed that the photocurrent decreased only 2.7% after storage of 2 months. These results indicate the satisfactory reproducibility, repeatability and stability of the biosensor towards UA sensing. The excellent stability of the biosensor might be mainly attributed to the strong binding of Fe_3O_4@C@MIT on MGCE, fast electron-transfer ability of carbon and rigid structure of MIT.

In order to demonstrate the feasibility of the UA biosensor for analytical application, the biosensor was employed to measure UA in urine sample. The recovery test was performed by spiking with different concentrations of UA to urine samples with 1000 times dilution. As showed in Table 1, with five different additions of UA to the urine samples containing 0.42 μM UA determined by the biosensor, the obtained recoveries ranged from 97.70% to 101.08%. The good recovery rate indicates that the UA biosensor is feasible for practical analysis. Table S1 presents the analysis results of UA in urine samples with the proposed method and HPLC. Good correlation is found between the two methods. Therefore, it is believed that a reliable biosensor has been obtained for UA determination in urine samples in our study.

Table 1
The recovery determination of UA in urine sample.

UA concentration (μM)		Recovery (%)
Added	Found[a]	
0.80	0.79 ± 0.04	98.75
6.00	6.03 ± 0.21	100.50
13.00	13.00 ± 0.36	100.00
20.00	19.54 ± 0.31	97.70
26.00	26.28 ± 1.05	101.08

[a] Average of three measurements ± S.D.

4. Conclusions

A novel UA photoelectrochemical biosensor was fabricated by a convenient attachment of Fe_3O_4@C@MIT on MGCE. The photoelectrochemical detection of UA exhibited high sensitivity, rapid response (<1s), wide linear range (0.3–34 μM), low detection limit (0.02 μM), good selectivity and stability. Detection of UA in urine sample was also performed with satisfactory results. The proposed biosensor showed a promising application in monitoring of biomolecules and open up a new avenue for the development of high selective and sensitive biosensor based on magnetic photocatalyst.

Acknowledgements

This work was supported by the National Natural Science Foundation of China (No. 51202059), the Research Foundation for Youth Scholars of Higher Education of Henan Province (No. 2013GGJS-047), the Key Foundation of Henan Educational Committee (No. 14A430014) and Foundation for Distinguished Young Scientists of Henan Polytechnic University (J2014-05) and the Opening Project of Henan Key Discipline Open Laboratory of Mining Engineering Materials (No. MEM13-4).

Appendix A. Supplementary material

Supplementary data associated with this article can be found in the online version at http://dx.doi.org/10.1016/j.bios.2014.10.013.

References

Chaudhari, R.D., Joshi, A.B., Srivastava, R., 2012. Sens. Actuators B 173, 882–889.
Chen, P.W., Vittal, R., Nien, P.C., Liou, G.S., Ho, K.C., 2010. Talanta 80, 1145–1151.
Guan, W.H., Duan, X.X., Reed, M.A., 2014. Biosens. Bioelectron. 51, 225–231.
Jeon, H.J., Choi, Y.K., Song, K.G., Lee, S.H., Yang, Y.H., Kim, H., Kim, S., Kumaran, R., Hong, S.W., Kim, H.J., 2013. Sens. Actuators B 185, 405–410.
Kaňďár, R., Drábková, P., Hampl, R., 2011. J. Chromatogr. B 879, 2834–2839.
Li, Y., Ran, G., Yi, W.J., Luo, H.Q., 2012. Microchim. Acta 178, 115–121.
Liu, G.G., He, F., Zhang, J., Li, L.J., Li, F.J., Chen, L.X., Huang, Y., 2014. Appl. Catal. B: Environ. 150–151, 515–522.
Luo, X.B., Deng, F., Min, L.J., Luo, S.L., Guo, B., Zeng, G.S., Au, C., 2013. Environ. Sci. Technol. 47, 7404–7412.
Miller, P., Oberholzer, V., 1990. Clin. Chem. 36, 668–669.
Piermarini, S., Migliorelli, D., Volpe, G., Massoud, R., Pierantozzi, A., Cortese, C., Palleschi, G., 2013. Sens. Actuators B 179, 170–174.
Pormsila, W., Krähenbühl, S., Hauser, P.C., 2009. Anal. Chim. Acta 636, 224–228.
Rahman, I.A., Vejayakumaran, P., Sipaut, C.S., Ismail, J., Chee, C.K., 2009. Mater. Chem. Phys. 114, 328–332.
Shi, H.J., Zhao, G.H., Liu, M.C., Zhu, Z.L., 2011. Electrochem. Commun. 13, 1404–1407.
Siekmann, L., 1985. J. Clin. Chem. Clin. Biochem. 23, 129–135.
Sun, B., Zhang, K., Chen, L.J., Guo, L.T., Ai, S.Y., 2013. Biosens. Bioelectron. 44, 48–51.
Sun, G.Q., Wang, P.P., Ge, S.G., Ge, L., Yu, J.H., Yan, M., 2014. Biosens. Bioelectron. 56, 97–103.
Tran., T., Li, T., Feng, J.Z., Cai, H., Yuan, J., Wang, L.J., Cai, Q.Y., N.Y., 2014. Sens. Actuators B 190, 745–751.
Tu, W.W., Dong, Y.T., Lei, J.P., Ju, H.X., 2010. Anal. Chem. 82, 8711–8716.
Wang, G.L., Jiao, H.J., Liu, K.L., Wu, X.M., Dong, Y.M., Li, Z.J., Zhang, C., 2014a. Electrochem. Commun. 41, 47–50.
Wang, G.L., Liu, K.L., Dong, Y.M., Li, Z.J., Zhang, C., 2014b. Anal. Chim. Acta 827, 34–39.
Wang, G.L., Xu, J.J., Chen, H.Y., Fu, S.Z., 2009. Biosens. Bioelectron. 25, 791–796.
Wang, Y.H., Zang, D.J., Ge, S.G., Ge, L., Yu, J.H., Yan, M., 2013. Electrochim. Acta 107, 147–154.
Yang, Z.P., Gong, X.Y., Zhang, C.J., 2010. Chem. Eng. J. 165, 117–121.
Yang, Z.P., Shang, X.G., Zhang, C.J., Zhu, J.P., 2014. Sens. Actuators B 201, 167–172.
Yang, Z.P., Yan, J.L., Zhang, C.J., Luo, S.Q., 2011. Colloids Surf. B 87, 187–191.
Yang, Z.P., Zhang, C.J., 2011. Biosens. Bioelectron. 29, 167–171.
Yang, Z.P., Zhang, C.J., 2013. Asia-Pac. J. Chem. Eng. 8, 54–58.
Zhang, B.T., Lu, L.L., Hu, Q.C., Huang, F., Lin, Z., 2014. Biosens. Bioelectron. 56, 243–249.
Zhang, X.R., Guo, Y.S., Liu, M.S., Zhang, S.S., 2013. RSC Adv. 3, 2846–2857.
Zhang, Z.P., Yin, J.G., 2014. Electrochim. Acta 119, 32–37.
Zhang, Z.Y., Kong, J.L., 2011. J. Hazard. Mater. 193, 325–329.